Chen, C., Liu, W., Li, F., Lin, C.-H., Liu, J., Pei, J., and Chen, Q. 2013. "A hybrid model for investigating transient particle transport in enclosed environments," *Building and Environment*, 62, 45-54.

A Hybrid Model for Investigating Transient Particle Transport in Enclosed Environments

Chun Chen[1], Wei Liu[2,1], Fei Li[2], Chao-Hsin Lin[3], Junjie Liu[2], Jingjing Pei[2*], Qingyan Chen[1,2]

[1] School of Mechanical Engineering, Purdue University, West Lafayette, IN 47907, USA
[2] School of Environmental Science and Engineering, Tianjin University, Tianjin 300072, China
[3] Environmental Control Systems, Boeing Commercial Airplanes, Everett, WA 98203, USA

* Address correspondence to Jingjing Pei, School of Environmental Science and Engineering Tianjin University, 92 Weijin Road, Naikai District, Tianjin, 300072, China.
Phone: 86-22-27403416; Fax: 86-22-27401561; * Email: jpei@tju.edu.cn

Abstract

It is important to accurately model person-to-person particle transport in mechanical ventilation spaces to create and maintain a healthy indoor environment. The present study introduces a hybrid DES-Lagrangian and RANS-Eulerian model for simulating transient particle transport in enclosed environments; this hybrid model can ensure the accuracy and reduce the computing cost. Our study estimated two key time constants for the model that are important parameters for reducing the computing costs. The two time constants estimated were verified by airflow data from both an office and an aircraft cabin case. This study also conducted experiments in the first-class cabin of an MD-82 commercial airliner with heated manikins to validate the hybrid model. A pulse particle source was applied at the mouth of an index manikin to simulate a cough. The particle concentrations versus time were measured at the breathing zone of the other manikins. The trend of particle concentrations versus time predicted by the hybrid model agrees with the experimental data. Therefore, the proposed hybrid model can be used for investigating transient particle transport in enclosed environments.

Keywords: Computational Fluid Dynamics (CFD); Detached Eddy Simulation (DES); Eulerian drift flux model; Lagrangian model; Aircraft Cabin; Office

Nomenclature

C_c	Cunningham coefficient caused by slippage
C_D	Drag coefficient
d_p	Particle diameter
d_0	Diameter of the mouth
$F(t)$	Airflow field of the room
$\vec{F}_a$	Other forces
$\vec{g}$	Gravitational acceleration vector
k	Turbulence kinetic energy
L	Distance from the mouth to a solid surface in the front
Q	Airflow rate
Re	Reynolds number
S_c	Generating rate of the particle source
s	Distance from the mouth
s^*	Distance that a cough can affect the surround flow
$s_{\overline{U_m}}$	Distance from the mouth corresponding to $\overline{U_m}$
t	Time
$t_{release}$	Duration of coughing
t_{decay}	Decay time when the $\overline{U_m}$ decreases to the surrounding value
t_{travel}	Traveling time needed for the coughing jet peak travel to position $s_{\overline{U_m}}$
$t_{DES\text{-}Lagrangian}$	Computing time when using DES-Lagrangian for the hybrid model
$t_{RANS\text{-}Eulerian}$	Computing time when using RANS-Eulerian for the hybrid model
$T_{hybrid}/T_{DES\text{-}Lagrangian}$	Ratio of the computing time by the hybrid model to the DES-Lagrangian model
$\vec{u}_a$	Velocity vector of air
u_j	Averaged fluid (air) velocity
$\vec{u}_p$	Velocity vector of the particle
u_{sj}	Gravitational settling velocity of particles
$U_m(s)$	Jet velocity at distance s
$\overline{U_m}$	Average velocity along the s^*
U_r	Reference room air velocity
U_0	Initial cough velocity
V	Volume of the room
η	Error
λ	mean free path of the air molecules
μ	Fluid viscosity
ξ_i	Normal random number
ρ	Air density
ρ_p	Particle density
τ	Room time constant
τ^*	Local time constant

τ_p	Particle relaxation time

1. Introduction

There is strong evidence of an association between indoor airflow patterns and the spread of infectious diseases, such as tuberculosis, influenza, and severe acute respiratory syndrome (SARS) [1]. Breathing, coughing, talking, and sneezing by an infected person can generate pathogen-carrying particles and can cause the transmission of infectious diseases [2-3]. Furthermore, infectious disease transmission in commercial aircraft cabins where passengers are in close proximity has become a major health issue [4]. Exhaled pathogen-containing particles generated by an infected passenger can disseminate throughout the cabin and cause infections in fellow passengers [5-6]. Therefore, it is important to accurately model the person-to-person particle transport in mechanical ventilated spaces in order to improve air distribution design to reduce the infection risk.

In recent years, Computational Fluid Dynamics (CFD) has been widely used in modeling airflow field and particle transport in enclosed environments, such as buildings [7], aircraft cabins [8], and hospital rooms [9]. For airflow modeling, there are several turbulence models such as Reynolds-Averaged Navier-Stokes (RANS) models, Large Eddy Simulation (LES), and Detached Eddy Simulation (DES), which have that has been reviewed and tested [10-11]. For particle modeling, Eulerian and Lagrangian are two popular methods. The Eulerian method often uses the drift flux model for considering the slippage between particle phase and fluid (air) phase. This model performed well in modeling indoor particle dispersion [12-14]. The Lagrangian method with the Discrete Random Walk (DRW) model has also performed very well in modeling and analyzing the particle transport and dispersion [15-17]. Most of the studies mentioned above focused on steady-state particle transport processes. However, particle transport processes can be in an unsteady state. Wang et al. [18] have tested different combinations of the airflow and particle models for steady- and unsteady-state cases. For steady-state airflow conditions, they preferred the RANS model with the Eulerian method due to the reasonable accuracy and low computing cost associated with the model. For unsteady-state airflow conditions, Wang et al. recommended the DES model with the Lagrangian method due to its relatively high accuracy. The reason for using DES rather than RANS model is that RANS model fails to predict correct transient airflow [11]. Moreover, when the airflow field is still developing, the Lagrangian method may have better accuracy than the Eulerian method since it accounts for more physics of airflow and particle motion [18]. But if the DES with Lagrangian model is applied for studying coughing, talking, and sneezing among persons in an enclosed environment, it requires considerable computing cost.

Thus, it is worthwhile to develop a model that can not only ensure the accuracy but also reduce the computing cost. It should be noticed that coughing, sneezing, or talking are unsteady-state and may have a significant impact on airflow distribution only in the first few seconds. But after the effect of the coughing, talking, and sneezing on the airflow is damped, the airflow can be regarded as steady-state. Then RANS with the Eulerian model can be applied to reduce the computing cost [18].

To further reduce the computing cost, one solution is to use a RANS model as the initial field for a DES model. Then the DES model can be used to calculate accurate results within a very short period of time. Now the question is how long the DES simulations should be performed in order to completely eliminate the effects of RANS modeling. In addition, if the DES is

applied to study coughing, how short should the transient simulation be so that the steady-state modeling afterwards will still give accurate results? This investigation set out to identify the two time constants and test the hybrid model for transient particle distributions in an airliner cabin.

2. Model determination

To identify the two time constants, this study used the RANS model for steady-state flows and the DES model for unsteady-state flows. Similar to in previous research, we used the Eulerian and Lagrangian methods for particle transport under steady-state and unsteady-state, respectively. This section details the flow and particle models used as well as the procedure to determine the two time constants.

2.1 Steady-state airflow conditions

2.1.1 Airflow and turbulence model

For steady-state flows, the renormalization group (RNG) k-ε model [19] is applied to calculate the airflow and turbulence. It has the best overall performance among all RANS models for enclosed environments [10]. The equations for RNG k-ε model can be found in the Fluent manual [20].

2.1.2. Particle transport model

For steady-state flows, the Eulerian drift flux model is applied to calculate the particle dispersion. The drift flux model considers the slippage between particle phase and fluid (air) phase, which takes the effect of the gravitational settling into consideration:

$$\frac{\partial[(u_j + u_{sj})C]}{\partial x_j} = \frac{\partial}{\partial x_j} \cdot (\frac{\upsilon_t}{\sigma_C} \frac{\partial C}{\partial x_j}) + S_C \tag{1}$$

where u_j is the averaged fluid (air) velocity; υ_t the turbulent kinetic viscosity; σ_c the turbulent Schimit number, which is usually equal to 1.0 [12]; and S_c the generating rate of the particle source. The u_{sj} in the equation is the gravitational settling velocity of the particles, which can be calculated by:

$$u_{sj} = \tau_p g_j \tag{2}$$

where τ_p is the particle relaxation time. The τ_p can be calculated by:

$$\tau_{\mathrm{p}} = \frac{\mathrm{C_c} \rho_{\mathrm{p}} {d_{\mathrm{p}}}^2}{18\mu} \tag{3}$$

where C_c is the Cunningham coefficient caused by slippage. The C_c can be calculated by [21]:

$$\mathrm{C_c} = 1 + \frac{\lambda}{d_p}(2.514 + 0.8 \times \exp(-0.55\frac{d_p}{\lambda})) \tag{4}$$

where λ is the mean free path of the air molecules.

2.2 Unsteady-state airflow conditions

2.2.1. Airflow and turbulence model

For unsteady-state flows, the DES Realizable k-ε model [22] is applied to predict the airflow and turbulence. The reason for using DES rather than RANS model for unsteady-state flows is that RANS model fails to predict correct transient airflow [11]. The equations for DES Realizable k-ε model can be found in the Fluent manual [20].

2.2.2. Particle transport model

For unsteady-state flows, the Lagrangian model is applied to calculate the particle dispersion. Using the momentum equation based on Newton's law, the trajectory of each particle can be calculated by:

$$\frac{d\vec{u}_p}{dt} = F_D(\vec{u}_a - \vec{u}_p) + \frac{\vec{g}(\rho_p - \rho_a)}{\rho_p} + \vec{F}_a \tag{5}$$

where $\vec{u}_p$ is the velocity vector of the particle; $\vec{u}_a$ the velocity vector of air; $\vec{g}$ the gravitational acceleration vector; ρ_p and ρ_a the particle and air density, respectively; and $\vec{F}_a$ Brownian motion and Saffman life force. The Brownian motion was included in the model since it is a typical characteristic of fine particles. Furthermore, the Saffman lift force may be relatively large near a room's wall for fine indoor particles [7]. Thus, we included the Saffman lift force in our study. The drag force is calculated by:

$$F_D(\vec{u}_a - \vec{u}_p) = \frac{18\mu}{\rho_p d_p^2}\frac{C_D \mathrm{Re}}{24}(\vec{u}_a - \vec{u}_p) \tag{6}$$

where μ is fluid viscosity, C_D the drag coefficient, Re Reynolds number, and d_p particle diameter.

The Discrete Random Walk (DRW) model [20] is used to model the turbulence dispersion:

$$u_i^{'} = \zeta_i\sqrt{2k/3} \tag{7}$$

where ξ_i is a normal random number, and k is turbulence kinetic energy.

2.3 Calculation procedure

2.3.1. Overall calculation procedure

In order to reduce the computing cost, this study introduces a hybrid DES-Lagrangian and RANS-Eulerian model to calculate the transient particle transport in enclosed environments. The key point of this model is to determine a suitable calculation procedure to keep the DES simulations as short as possible without sacrificing the accuracy.

Figure 1 shows the overall calculation procedure for using the hybrid DES-Lagrangian and

RANS-Eulerian models, taking coughing as an example. It consists of three steps:

(1). The RNG k-ε model is used to calculate the initial field of airflow under steady-state conditions. Then the DES Realizable k-ε model is used to calculate for a period of time, t_1, as shown in Figure 1 to obtain the time-dependent flow distribution under steady-state boundary conditions;

(2). The DES-Lagrangian model is applied to calculate for another period of time, t_2, also shown in the figure for the unsteady-state boundary conditions due to coughing;

(3). The RANS-Eulerian model is used again to calculate flow fields under the steady-state boundary conditions, by assuming the effect of the coughing on the airflow distribution being fully damped.

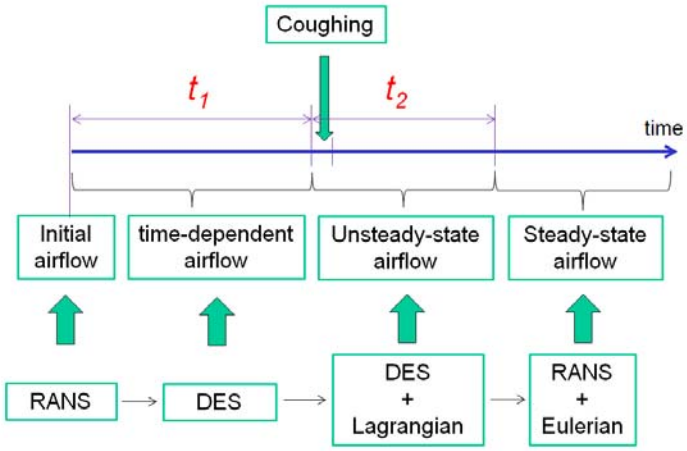

Figure 1. Overall calculation procedure.

The above procedure shows that the computing effort depends very much on the t_1 and t_2. The shorter of the t_1 and t_2 are, the less the computing effort should be since transient DES-Lagrangian calculations are very computationally intensive. The following subsection describes our effort in estimating the t_1 and t_2.

2.3.2. Estimation for t_1

The estimation of t_1 started from the room time constant, τ. Normally, a flow will become stable again after the corresponding boundary conditions have been changed and stabilized for 2τ [11]. Therefore, if we start to simulate room airflow with a uniform initial field by using the DES model, the results of the first 2τ period are considered to be transient from its initial field to a stable one. However, this study did not use the DES model with a uniform initial field, but rather a flow field obtained from the RANS model. Although the flow field may not be accurate, it should be close to reality, $t=t^*$, as shown in Figure 2. Then the DES model should only be used for the $t_1 = 2\tau - t^*$ period to reach a stable airflow field.

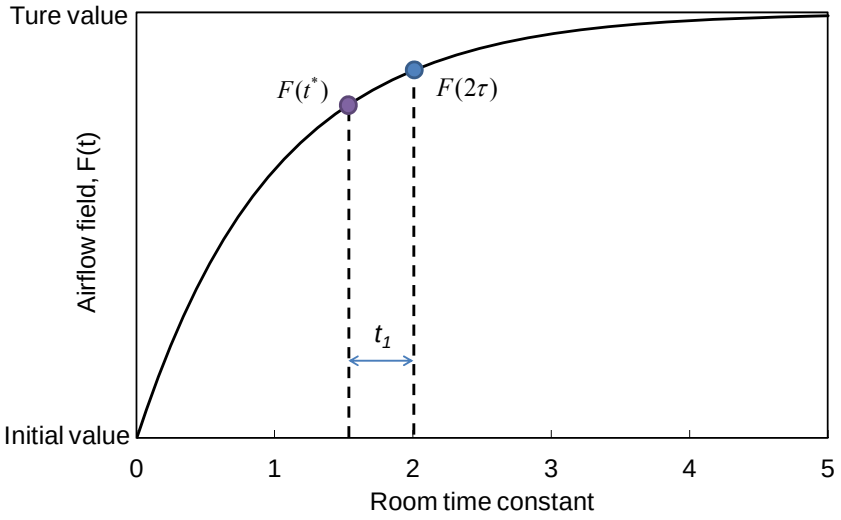

Figure 2. Airflow field versus room time constant for estimating t_1.

Let us define an error between $F(t^*)$ and $F(2\tau)$ as η, then the following equation can be obtained:

$$\frac{F(t^*)}{F(2\tau)} = \frac{(1-e^{-\frac{t^*}{\tau}})}{(1-e^{-\frac{2\tau}{\tau}})} = 1-\eta \tag{8}$$

Therefore, the t_1 can be calculated by:

$$t_1 = 2\tau - t^* = [2 - \ln\frac{1}{1-(1-\eta)(1-e^{-2})}]\tau \tag{9}$$

If we use the typical error between the RANS and DES model, η, to be 10% as suggested by Wang [23], the t_1 is obtained as,

$$t_1 = 0.5\tau \tag{10}$$

2.3.3. Estimation for t_2

The t_2 is the time period when a cough can affect the room airflow distribution and the flow is considered to be unsteady. It should be noted that the time-dependent air velocity varies along the traveling path of the coughing jet. To estimate the overall process, this study averaged the coughing jet peak velocity along the traveling path, $\overline{U_m}$, and investigated its decay process.

Figure 3 shows an example of the air velocity versus time at position $s_{\overline{U_m}}$. $s_{\overline{U_m}}$ is the corresponding distance from the mouth to $\overline{U_m}$. As shown in the figure, the t_2 is affected by:

(1). The duration of the coughing ($t_{release}$);

(2). The traveling time needed for the coughing jet peak to travel to position $s_{\overline{U_m}}$ (t_{travel}).

(3). The decay time when the $\overline{U_m}$ decreases to the surrounding value (t_{decay});

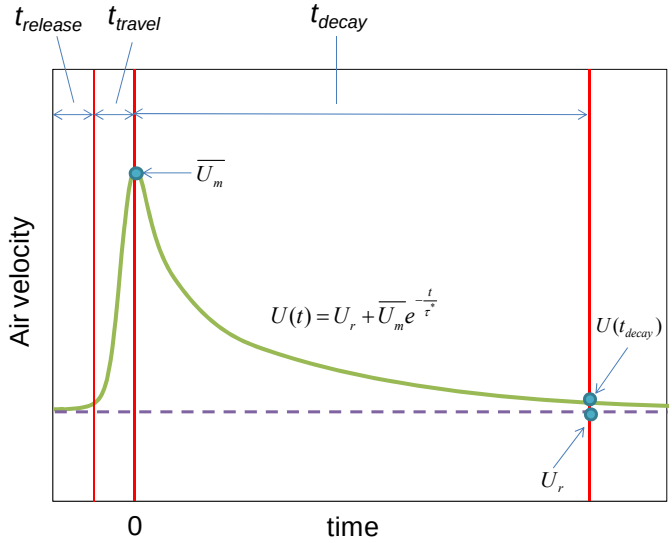

Figure 3. An example of the air velocity versus time at position $s_{\overline{U_m}}$.

The duration of coughing, $t_{release}$, has been studied by many researchers. For example, Gupta et al. [24] found the time to be

$$t_{release} = 0.4 \text{ s} \tag{11}$$

by measuring it from 25 human subjects.

To estimate the $\overline{U_m}$, this study referred to the jet equation [25]:

$$U_m(s) = \begin{cases} U_0, & s < 6.8d_0 \\ \dfrac{6.8U_0 d_0}{s}, & s \geq 6.8d_0 \end{cases} \tag{12}$$

where $U_m(s)$ is the jet velocity at distance s, U_0 the coughing initial velocity, d_0 the diameter of the mouth, and s the distance from the mouth. It should be noted that the above jet equation is for steady-state, while the coughing jet is unsteady with a decay process. The $U_m(s)$ in the jet equation can be regarded as the coughing jet peak at distance s. Then the $\overline{U_m}$ can be determined via:

$$\overline{U_m} = \frac{1}{s^*}\int_0^{s^*} U_m(s)ds = \frac{6.8U_0 d_0}{s^*}\left(1 + \ln\frac{s^*}{6.8d_0}\right) \tag{13}$$

where s^* is the distance that a cough can travel. This study assumed that when the centerline velocity decays to a reference room air velocity, the effect of the coughing is damped. The reference room air velocity, U_r, was set as 0.25 m/s, which is a recommended limit value for thermal comfort [26]. Then, the s^* can be calculated using the jet equation. However, in many

enclosed environments, the jet is not a free one but an impinging one. The distance from the mouth to the wall is L and $L<s^*$, then the s^* should be set as L, namely:

$$s^* = \min(\frac{6.8U_0 d_0}{U_r},\ L) \tag{14}$$

Based on Eq. (12), the distance from the mouth corresponding to $\overline{U_m}$ can be calculated by:

$$s_{\overline{U_m}} = \frac{6.8U_0 d_0}{\overline{U_m}} \tag{15}$$

Based on Eqs. (12) and (15), the traveling time, t_{travel}, can be calculated by integrating the coughing jet peak traveling time from the mouth to the position $s_{\overline{U_m}}$:

$$t_{travel} = \int_0^{s_{\overline{U_m}}} \frac{1}{U_m(s)} ds = \frac{6.8d_0}{U_0} + \frac{s_{\overline{U_m}}^2 - (6.8d_0)^2}{13.6U_0 d_0} \tag{16}$$

The decay time, t_{decay}, is the time needed for the $\overline{U_m}$ to diminish to the surrounding velocity. The jet velocity at position $s_{\overline{U_m}}$ during the decay process can be described by:

$$U(t) = U_r + \overline{U_m} \cdot e^{-\frac{t}{\tau^*}} \tag{17}$$

where U_r is the reference room air velocity, τ^* is the average local time constant. This study simply considered the local time constant as the time needed for the coughing jet peak to diminish along its traveling path. Based on Eqs (12) and (14), the τ^* can be determined by:

$$\tau^* = \int_0^{s^*} \frac{1}{U_m(s)} ds = \frac{6.8d_0}{U_0} + \frac{s^{*2} - (6.8d_0)^2}{13.6U_0 d_0} \tag{18}$$

As shown in Figure 3, if the average coughing jet peak velocity decreases to a value $U(t_{decay})$ that is very close to the reference room air velocity, U_r, the decay process is considered to be completed. Let us define an error between $U(t_{decay})$ and U_r as η, then the following equation can be obtained:

$$\eta = \frac{U(t_{decay}) - U_r}{U_r} = \frac{\overline{U_m}}{U_r} e^{-\frac{t_{decay}}{\tau^*}} \tag{19}$$

Reformatting Eq. (19), the decay time can be obtained:

$$t_{decay} = \ln(\frac{\overline{U_m}}{\eta U_r})\tau^* \tag{20}$$

Then the t_2 can be roughly estimated by combining Eqs. (11), (16) and (20):

$$t_2 = t_{release} + t_{travel} + t_{decay} \quad (21)$$

3. Verification of the two time constants used in the hybrid model

3.1 Verification of t_1

This study used two cases to verify the t_1 proposed in the previous section. The first case was in an office with an Under-Floor Air-Distribution (UFAD) system [15], as shown in Figure 4. The room had four heated human simulators. The air was supplied from the two floor inlets and exhausted from the ceiling. The air velocity was measured at the seven poles (V1 to V7) as shown in the figure. The second one was in a four-row aircraft cabin mockup [16], as shown in Figure 5. The cabin mockup had 28 seats, 14 of which were occupied by heated human simulators. The air was supplied from two groups of linear diffusers located near the center of the ceiling. The air velocity vectors were measured in the cross-section through the third row and the mid-section along the longitudinal direction. The air change rates of the office and the cabin were 5.5 and 24 ACH, respectively. The corresponding room time constants were 655 and 150 s, respectively. Since the estimation of the t_1 is directly associated with the room time constant, the two cases with quite different room time constants are useful to verify the t_1 estimated in the previous section.

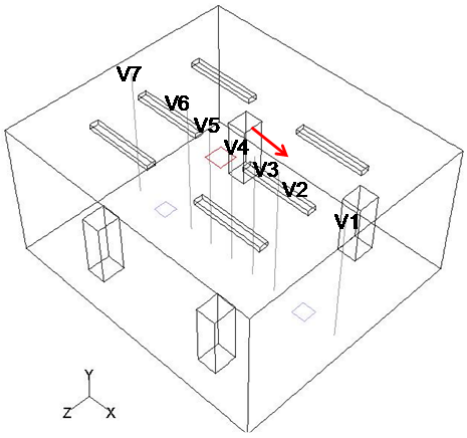

Figure 4. Schematic of the office with UFAD system where air velocity was measured at the seven poles [15].

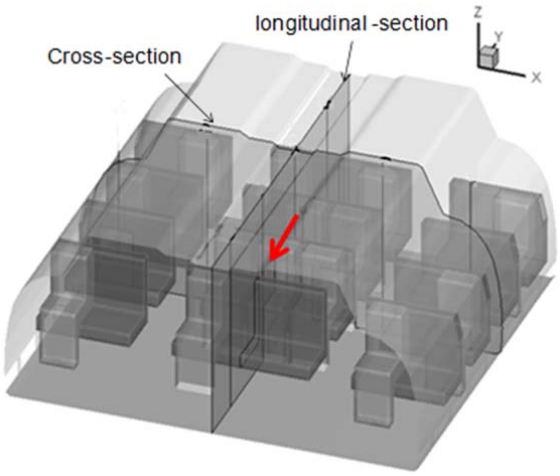

Figure 5. Schematic of the four-row aircraft cabin mockup [16].

Since the t_1 was associated with both the RANS and DES models, this study used the following four approaches to calculate the airflow fields of these two cases:

(1). Approach_1: only RANS model,
(2). Approach_2a: combined RANS and DES with $t_1=0.5\tau$,
(3). Approach_2b: combined RANS and DES with $t_1=2\tau$,
(4). Approach_3: only DES model,

Approach_2a averaged the results between 0.5τ and 1.5τ as the mean flow field, which was the approach proposed in the previous section. Similarly, Approach_2b averaged the results between 2τ and 3τ as the mean flow field. When Approach_3 was used, the investigation calculated the airflow fields for 2τ with a uniform initial flow field and then averaged the results between 2τ and 3τ to obtain the mean flow field. Since normally a flow will become stable again after the corresponding boundary conditions have been changed for 2τ, we expected that both Approach_2b and Approach_3 could provide an accurate airflow field as a benchmark.

Figure 6 compares the air velocities obtained by the different approaches with the experimental data from Zhang and Chen [15] for the office case. Approach_1 and Approach_3 performed similarly at poles V3 to V6. Approach_1 matched better with the experimental data in the middle part of pole V1, but worse at the lower part of pole V1 and middle part of pole V2 than in Approach_3. At pole V7, both the approaches showed significant discrepancies from the experimental data. Therefore, it is difficult to say which approach is better for predicting the airflow field in this case. Since the DES model can provide detailed information on transitional flows, this study used Approach_3 as the benchmark. As shown in the figure, Approach_2b agreed very well with Approach_3. This further confirms that Approach_3 can be used as the benchmark. To verify the t_1 proposed in the previous section, this investigation compared Approach_2a with Approach_3. The results show that they matched very well for the whole field. Although Approach_2a still showed significant discrepancies from the experimental data, it can at least achieve the similar accuracy to Approach_3. Hence, $t_1=0.5\tau$ was long enough to obtain the accurate time-dependent flow distribution under steady-state boundary conditions. This study has correctly estimated the t_1 for the office case.

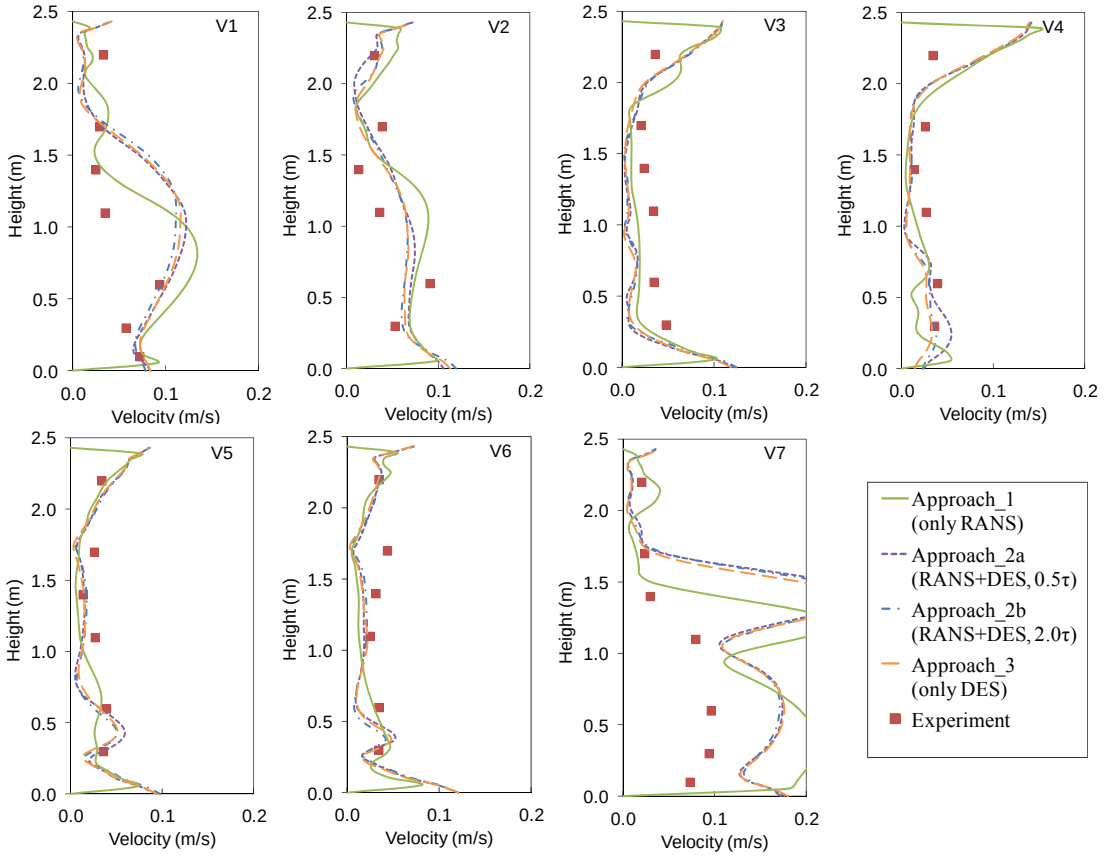

Figure 6. Comparison of air velocities obtained by the different approaches with the experimental data from Zhang and Chen [15].

Figure 7 compares the airflow fields obtained by the different approaches with the experimental data from Zhang et al. [16] for the cabin case. For easy observation, only Approach_2a and Approach_3 were shown in the Figure. It can be seen that Approach_3 showed significant discrepancies from the experimental data. Zhang et al. [16] also reported this phenomenon and concluded that the modeling results were very sensitive to the accuracy of the boundary conditions. It should be noted that the velocity directions at the inlets were not measured in the experiments, which may generate errors for quantitative comparison. Nevertheless, the experimental data still preserved the qualitative character of the airflow field. Similar to in the office case, this investigation used Approach_3 as the benchmark. To verify the t_1 proposed in the previous section, this study compared Approach_2a with Approach_3. In the mid-section along the longitudinal direction, both the approaches predicted an upward motion of the airflow field. The quantitative comparison also showed very good agreement in this section. In the cross-section through the third row, both the approaches again matched well with each other for most of the positions. Although differences can be found at some positions at the upper left side of this section, the general airflow pattern was similar between the two approaches. Generally speaking, Approach_2a agreed well with Approach_3. Thus, $t_1=0.5\tau$ is a reasonable estimate for the cabin case.

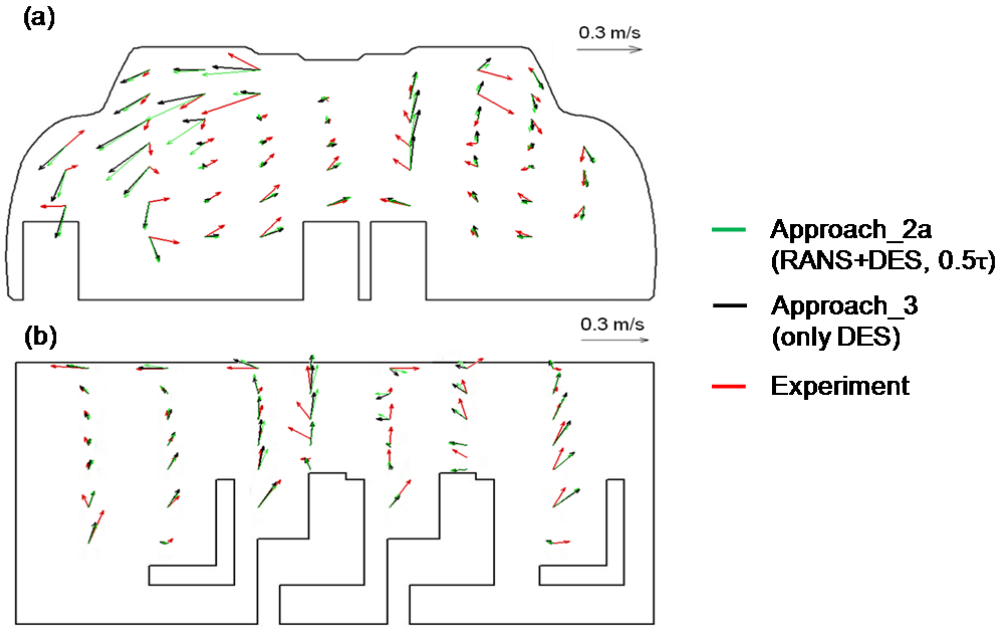

Figure 7. Comparison of airflow field obtained by the different approaches with the experimental data from Zhang et al. [16]: (a) cross-section through the third row, (b) mid-section along the longitudinal direction.

The two cases with different room time constants show that the t_1 estimated by Eq. (10) is acceptable. The t_1 can be used as the minimum time for obtaining an accurate flow field by DES if the calculation starts from a RANS result.

3.2. Verification of t_2

This investigation again used the office and the aircraft cabin cases to verify t_2. Different from t_1, t_2 was only associated with the DES model. Sub-section 3.1 has shown that the DES model can be used as a benchmark. Hence, the DES model was used to calculate the jet velocity versus time at different positions. Then the time needed for the jet velocity decreased to the surrounding value can be obtained from the DES results as a benchmark to verify the t_2 proposed. The arrows in Figures 4 and 5, respectively, show the mouth location and coughing direction. Table 1 lists the input parameters and the estimated t_2. According to Eq. (12), the jet was associated with the coughing velocity (U_0) and the diameter of the mouth (d_0). The U_0 was set as 8 m/s for both cases, while the d_0 was set as 4 and 1 cm for the office and cabin cases, respectively, to create jets with different characteristics. The two cases with different jet characteristics are useful to verify the t_2 estimated in the previous section.

Table 1. Input parameters and the t_2 estimated.

Case	U_0	d_0	L	η	$t_{release}$	t_{travel}	t_{decay}	t_2
	m/s	m	m	--	s	s	s	s
Office (UFAD)	8	0.04	2.10	5%	0.4	0.13	5.70	6.22
Aircraft Cabin	8	0.01	0.65	5%	0.4	0.04	2.11	2.55

Figure 8 shows the results of the jet velocity versus time at different positions from the DES model for both the office and cabin cases. It can be seen from the table that the influence of the t_{decay} on the t_2 was dominating for both the office and cabin cases. This was supported by

the DES model calculation as shown in Figure 8. The t_2 was estimated to be 6.22 and 2.55 s through Eq. (21) for the office and cabin cases, respectively. The estimated t_2 for the office case was larger than the cabin case, which was also supported by the DES modeling results. As shown in Figure 8(a), after the estimated t_2, 6.22 s, the air velocity had decreased to the surrounding value for the office case. Similarly, after the estimated t_2, 2.55 s, the air velocity had decreased to the surrounding value for the cabin case, as shown in Figure 8(b). The two cases with different jet characteristics show that the t_2 estimated by Eq. (21) is acceptable. Hence, the t_2 can be used as the minimum time in which a cough can affect the room airflow distribution.

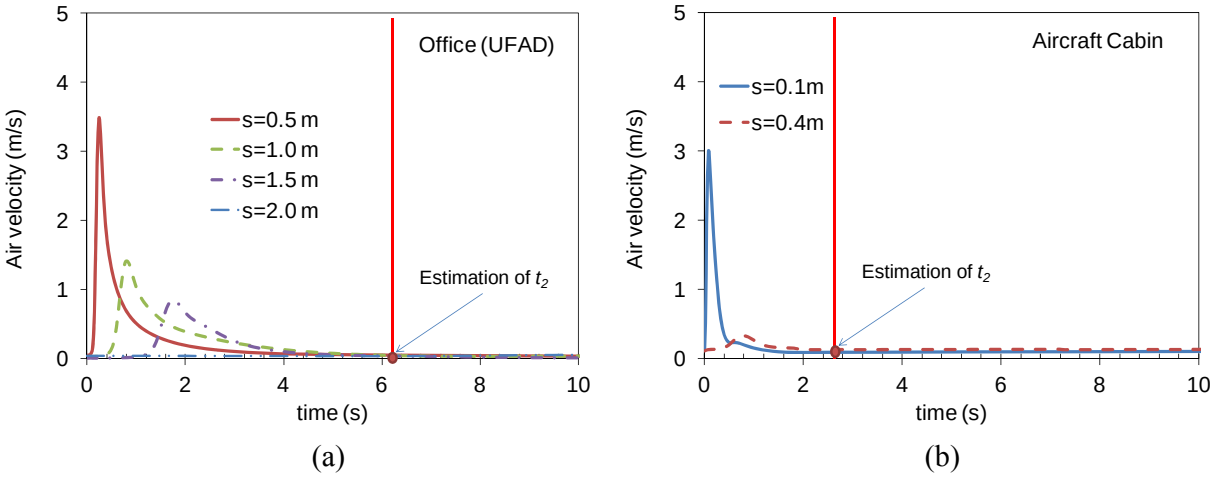

(a) (b)

Figure 8. Jet velocity versus time from DES model and estimated t_2 for (a) office and (b) aircraft cabin case.

4. Validation of the hybrid model

With the calculation procedure as shown in Figure 1 and the two time constants as determined by Eqs. (10) and (21), this investigation used the hybrid model for predicting the transient particle concentration distribution in the first-class cabin of an MD-82 aircraft cabin. The cabin was fully-occupied by manikins and mechanically ventilated. The case was an ideal one for studying person-to-person transient particle transport in a mechanical ventilated space. Since we have conducted experimental measurements of transient particle distribution in the cabin, the data can be used to validate the hybrid model. This section details our effort in the model validation.

4.1 Experimental setup

Figure 9(a) shows the schematic model of the fully-occupied first-class cabin of the MD-82 aircraft. The cabin contained three rows of seats, and each row had four seats as numbered in Figure 9(b). A detailed description of the cabin can be found in Liu et al. [27]. The heated manikins were built by wrapping solid manikins with nickel-chromium wires. The sensible heat production of the manikin was 75 W [28]. The airflow and thermal boundary conditions of the first-class cabin were measured previously by Liu et al. [27-28].

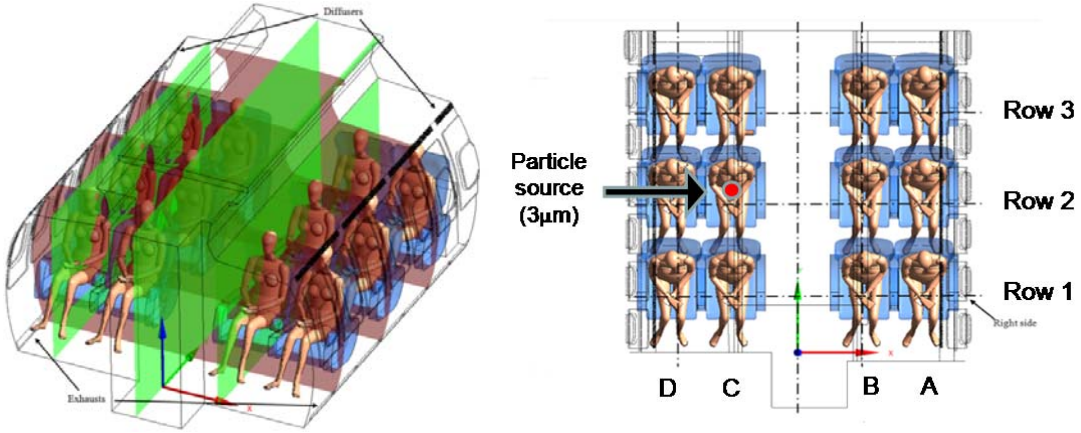

(a) (b)

Figure 9. Schematic of the fully-occupied first-class cabin: (a) perspective view and (b) plane view [28]

The manikin 2C was set as the index passenger with a particle source. At the mouth, particles were released to the cabin air through a tube of 0.01 m in diameter at a speed of 1.03 ± 0.02 m/s. Although the speed was different from a real cough, the experiment was still meaningful since the aim of this study was to provide reliable experimental data to validate the hybrid model. To simulate a cough, an electromagnetic valve was installed in the tube. Then the particle release time could be controlled. A MAG 3000 PALAS particle generator was used to generate Di-Ethyl-Hexyl-Sebacat (DEHS) mono-size particles with a diameter of 3 μm. DEHS is a non-soluble liquid with a low evaporation rate and a density of 912 kg/m^3.

The particle concentrations versus time at the breathing zones were measured in front of each passenger's mouth. An aerodynamic particle sizer (APS 3321, TSI Inc., St. Paul, MN) spectrometer was used to measure the particle concentration. To measure the transient particle concentration in a location, the sampling time should be larger than the response time of the aerodynamic particle sizer but should also be as short as possible. The response time of the instrument was 1 s so it was used in the experiment. Since only one particle sizer spectrometer was available, the particle concentrations versus time were measured for one passenger at a time. The measurement time for each passenger was set as 500 s, so the entire experiment for measuring 11 passengers took about 2 hours. The complete experiment was repeated 3 times on different days. Since the experimental data quality is related to the repeatability of the experiment, Figure 10 compares the three independent measurements of particle concentration versus time, taking 1B and 2A as examples. It can be seen that the three independent measurements matched very well with each other. Hence, the repeatability of the experiment is acceptable.

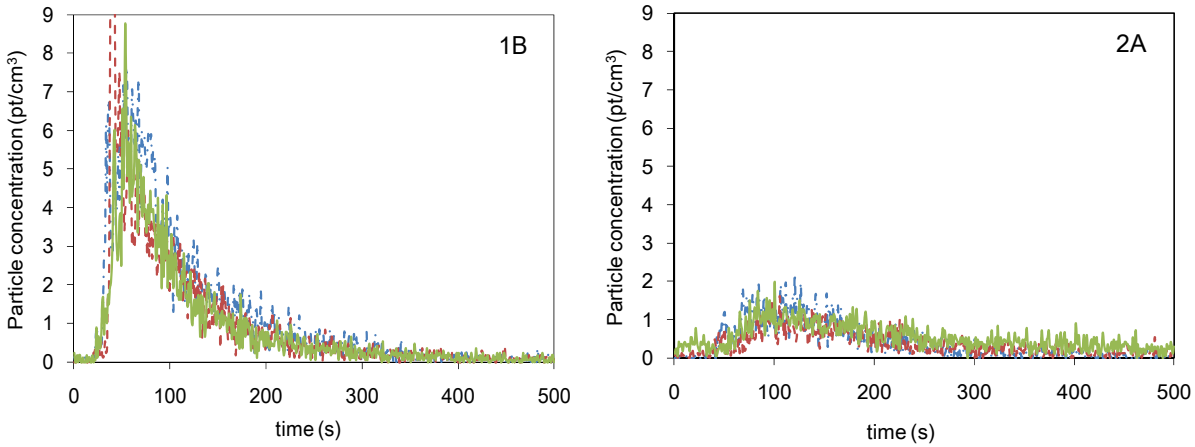

(a) (b)

Figure 10. Comparison of three independent measurements of particle concentration versus time for (a) 1B and (b) 2A.

The source release time is also an important factor of experimental data quality. A single cough lasts for less than 1 s [23]. With such a short source release time in the experiment, the particle concentrations in the cabin may be too low to be detected by the aerodynamic particle sizer, so the data quality would be poor. Therefore, the source release time should be increased to some extent. Although the increased source release time was different from the real coughing case, the experiment was still meaningful since the aim of this study was to provide reliable experimental data to validate the hybrid model. If the source release time had been too long, the experiment might have become a steady-state case. Hence, the source release time still needs to be as short as possible to meet the purpose of this study, while the particle concentrations at the breathing zone of other manikins should be detectable with the aerodynamic particle sizer. This investigation compared the particle concentration versus time at 1A and 2A under three different source release times: 5, 20, and 60 s, as shown in Figure 11. It can be seen that a 5 s source release time cannot result in obvious particle concentration peaks. A 20 s source release time can generate a peak concentration that is more than 5 times the background concentration. Although a 60 s source release time can result in even higher peaks, this may be too long for a transient particle transport case. Hence, a 20 s source release time was applied in the experiment.

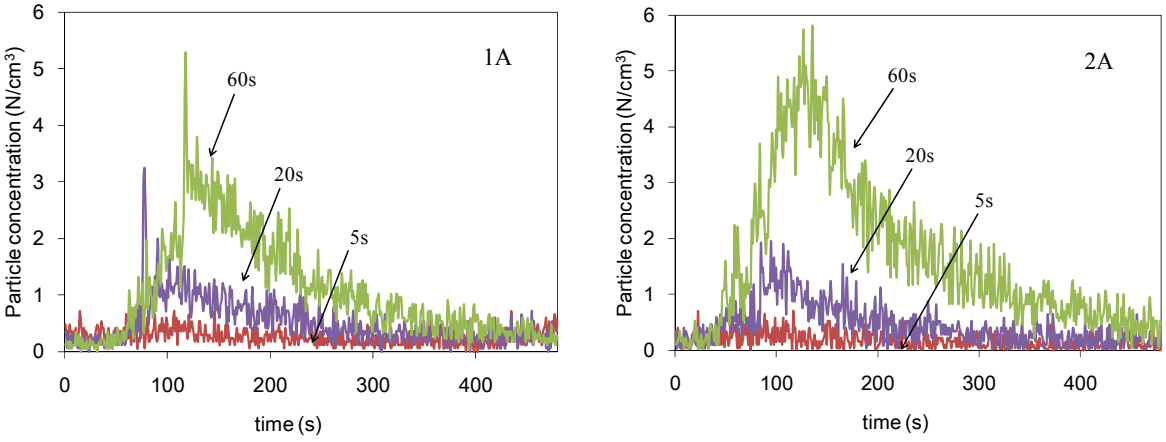

(a) (b)

Figure 11. Comparison of the particle concentration levels when the source release time was 5, 20, and 60 s for (a) 1A and (b) 2A.

4.2 Validation

The hybrid model was then used to calculate the transient particle distribution in the first-class cabin of the MD-82 aircraft by using the digital geometry model as shown in Figure 9. The numerical simulation was conducted using the CFD code ANSYS Fluent 12.1. The user-defined function (UDF) was implemented to realize the Eulerian drift flux model. Three grid resolutions (6.4, 8.4, and 13 million) were tested for CFD grid independence. The 6.4 million grid resolution was sufficiently fine to capture such a flow. When using the Lagrangian method, 500,000 particles with a diameter of 3 μm were generated during the 20 s source release time. The particle source in-cell (PSI-C) scheme [15] was used to translate the trajectories into the concentrations. The time step was set at 0.02 s. The particle deposition was neglected in the simulations due to the large air change rate in the aircraft cabin [8]. The t_1 and t_2 was estimated to be 51 and 22.3 s by using Eqs. (10) and (21), respectively, for the cabin.

Figure 12 compares the numerical results of the transient particle concentrations at the breathing zone of each passenger with the corresponding experimental data. For easy observation, the experimental data were averaged every 15 s. Since the experiment was repeated 3 times, each solid point in the figure represents the average value of the 45 data points (15×3=45). The lower and upper bound of the error bars represents the 10^{th} and 90^{th} percentile of the 45 data points, respectively. The experimental data and modeling results were normalized by the maximum concentration among the monitoring points for the entire experiment. The comparison in Figure 12 shows that the trend of the particle concentration variation versus time predicted by the hybrid model agrees with the experimental data.

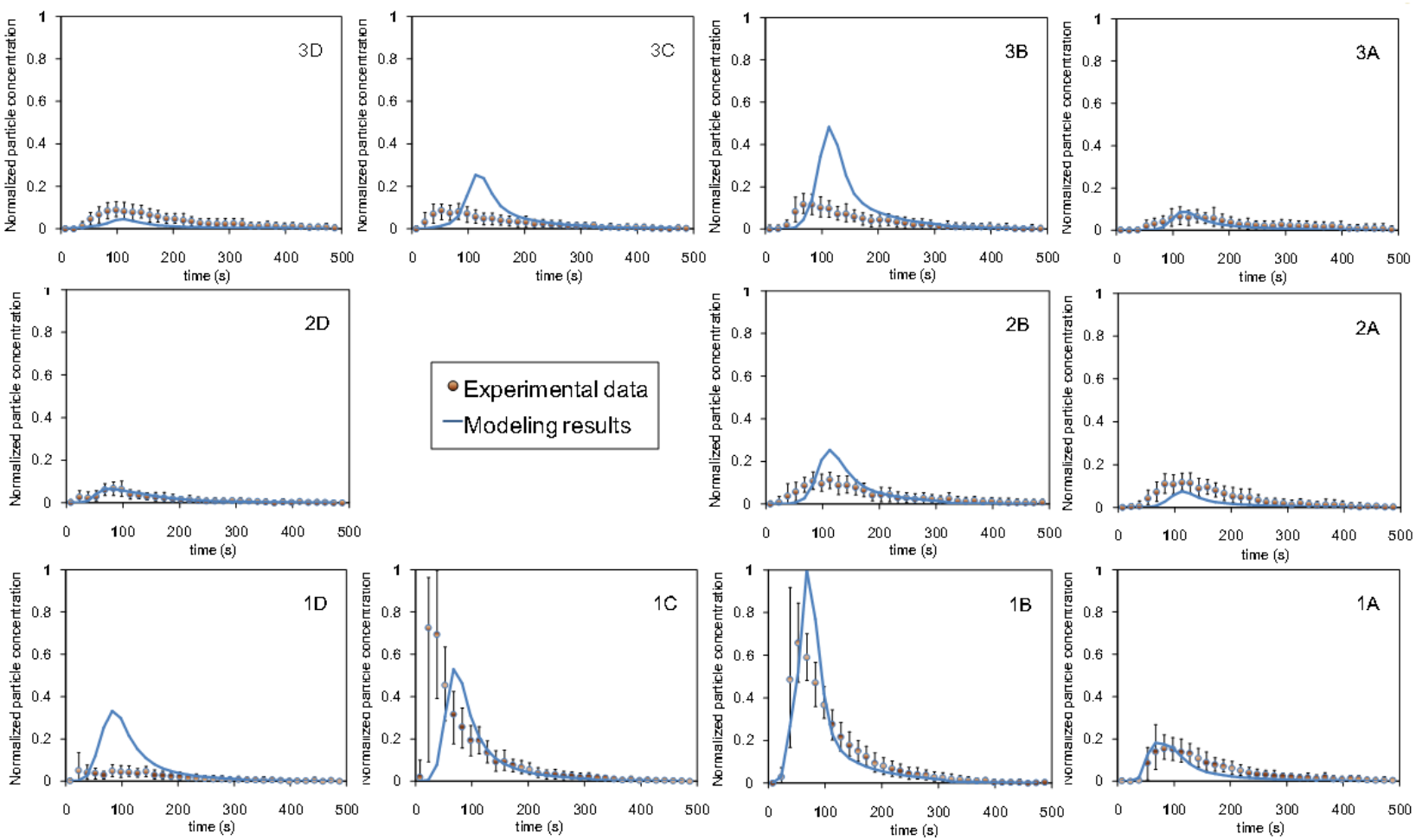

Figure 12. Comparison of the numerical results of transient particle concentrations at the breathing zone of each manikin with the corresponding experimental data. The experimental data and modeling results were normalized by the maximum concentration among the monitoring points for the entire experiment.

Note that a large portion of the released particles moved forward from 2C to 1B, and 1C and resulted in relatively high peak concentrations. The rest of the particles dispersed to other locations and also led to peaks but with lower concentrations. The hybrid model over-predicted the concentrations at 1D, 3B, and 3C and somewhat under-predicted at 1C. We suspected that the discrepancies were mainly attributed to the differences between the modeled and measured airflow fields, as shown in Figure 13. Observing the experimental data, very limited portion of particles moved backward, which indicated that the general direction of the airflow above 2C was pointing forward. However, the modeled airflow showed the existence of both the forward and backward directions. Therefore, the modeling results showed that a considerable portion of particles moved backward so that the concentrations at 3B and 3C increased. The airflow distribution in aircraft cabins is extremely complicated and difficult to model accurately [16, 27-28]. Nevertheless, the hybrid model can predict the transient particle concentration distribution for engineering applications.

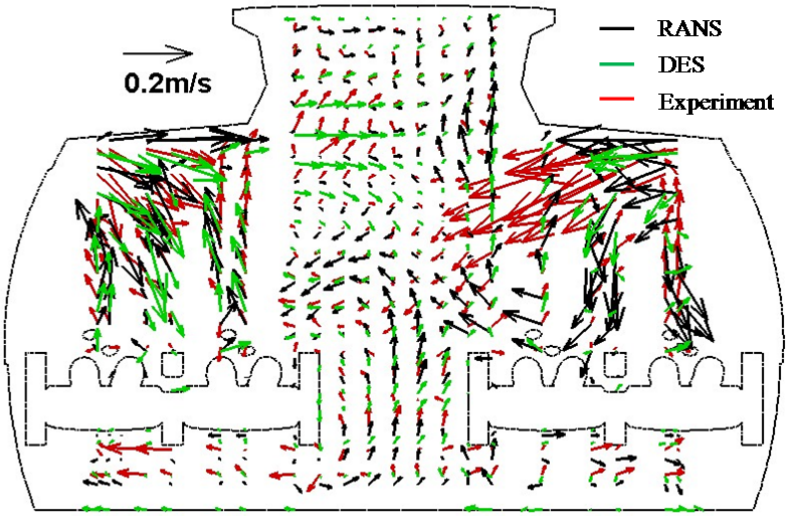

Figure 13. Comparison of the numerical results of the air velocity vectors with the experimental data from Liu et al. [28] at the cross-section through the third row.

5. Discussion

The validation section has shown that the hybrid model is acceptable for engineering applications. In addition, the hybrid model can significantly reduce the computing cost in two aspects. First, the traditional approach for obtaining the time-dependent flow distribution using the DES model is Approach_2b or Approach_3. However, the hybrid model uses Approach_2a, which can save about 75% of the computing time compared with Appraoch_2b or Approach_3. Secondly, Wang et al. [18] recommended using the DES-Lagrangian model for transient particle transport simulations. The hybrid model uses the DES-Lagrangian model in the first few seconds of the flow time and the RANS-Eulerian model afterwards. The RANS-Eulerian model can save about 84% of the computing time compared with the DES-Lagrangian model [18]. The ratio of the computing time by the hybrid model to the DES-Lagrangian model is:

$$\frac{T_{hybrid}}{T_{DES-Lagrangian}} = \frac{t_{DES-Lagrangian} + (1-84\%)\cdot t_{RANS-Eulerian}}{t_{DES-Lagrangian} + t_{RANS-Eulerian}} \tag{22}$$

where $t_{DES\text{-}Lagrangian}$ and $t_{RANS\text{-}Eulerian}$ is the computing time used by DES-Lagrangian and RANS-Eulerian, respectively, for the hybrid model. Taking the first-class cabin of the MD-82 aircraft as an example, the $t_{DES\text{-}Lagrangian}$ and $t_{RANS\text{-}Eulerian}$ were 22.3 and 477.7 s, respectively. Then $T_{hybrid}/T_{DES\text{-}Lagrangian}$ was only 20%; that is, the hybrid model can save about 80% of the computing time compared with the DES-Lagrangian model. Therefore, the proposed hybrid model can significantly reduce the computing costs.

It should be noticed that a person who is very ill with a respiratory infection tends to cough more than just once. To take this factor into account, the supper-imposition method proposed by Gupta et al. [29] can used together with our experimental or modeling data to estimate the effect of multiple coughs. Furthermore, a lot of people attempt to cover their mouth with their hand or a tissue when they cough. However, a model for predicting exhaled particle transport by coughs with covering the mouth with a hand or tissue is not available, which deserves further investigations. Our study simulated a scenario when a coughing passenger who was at sleep so he/she could not cover the mouth when coughing.

6. Conclusions

This study proposed a hybrid DES-Lagrangian and RANS-Eulerian model for investigating transient particle transport in enclosed environments. From the results presented in this paper, the following conclusions can be made:

(1). This study proposed how to estimate the two key time constants for the model, t_1 and t_2. The estimated t_1 and t_2 were verified by an office and an aircraft cabin case.

(2). This investigation conducted experimental measurements of transient particle distributions in the first-class cabin of an MD-82 aircraft cabin to validate the hybrid model. The results show that the model can predict the trend of the transient particle concentration distribution when compared with the experimental data.

(3). The proposed hybrid DES-Lagrangian and RANS-Eulerian model can be used for investigating transient particle transport in enclosed environments with relatively high accuracy, while the computing time can be reduced by 80%.

Acknowledgement

The research presented in this paper was partially supported by the National Basic Research Program of China (The 973 Program) through grant No. 2012CB720100 and by the International Science and Technology Collaboration Program of Tianjin Commission of Science and Technology through grant No. 10ZCGHHZ00900. The authors would like to thank Chen Shen and Jianmin Li of Tianjin University for their help in the experiment.

References

[1] Li Y, Leung GM, Tang JW, Yang X, Chao C, Lin JH, Lu JW, Nielsen PV, Niu JL, Qian H, Sleigh AC, Su HJ, Sundell J, Wong TW, Yuen PL. Role of ventilation in airborne transmission of infectious agents in the built environment – a multidisciplinary systematic review. Indoor Air 2007; 17: 2–18.

[2] Nicas M, Nazaroff WW, Hubbard A. Toward understanding the risk of secondary airborne infection: Emission of respirable pathogens. J Occup Environ Hyg 2005; 2: 143–154.

[3] Morawska L. Droplet fate in indoor environments, or can we prevent the spread of infection? Indoor Air 2006; 16: 335–347.

[4] Olsen SJ, Chang H, Cheung TY, Tang AF, Fisk TL, Ooi SP, Kuo H, Jiang DD, Chen K, Lando J, Hsu K, Chen T, Dowell SF. Transmission of the severe acute respiratory syndrome on aircraft. New Eng J Med 2003; 349: 2416-2422.

[5] Mangili A, Gendreau MA. Transmission of infectious disease during commercial air travel. Lancet 2005; 365: 989-996.

[6] Moser MR, Bender TR, Margolis HS, Noble GR, Kendal AP, Ritter DG. An outbreak of influenza aboard a commercial airliner. Am J Epi 1979;110: 1-6.

[7] Zhao B, Zhang Y, Li X, Yang X, Huang D. Comparison of indoor aerosol particle concentration and deposition in different ventilated rooms by numerical method. Build Environ 2004; 39: 1-8.

[8] Gupta JK, Lin C-H, Chen Q. Transport of expiratory droplets in an aircraft cabin. Indoor Air 2011; 21: 3-11.

[9] Chen C, Zhao B, Cui W, Dong L, An N, Ouyang X. The effectiveness of an air cleaner in controlling droplet/aerosol particle dispersion emitted from a patient's mouth in the indoor environment of dental clinics. J R Soc Interface 2010; 7: 1105-1118.

[10] Zhang Z, Zhai ZQ, Zhang W, Chen Q. Evaluation of various turbulence models in predicting airflow and turbulence in enclosed environments by CFD: part 2 - comparison with experimental data from literature. HVAC&R Res 2007; 13: 871-886.

[11] Wang M, Chen Q. Assessment of various turbulence models for transitional flows in enclosed environment. HVAC&R Res 2009; 15: 1099-1119.

[12] Murakami S, Kato S, Nagano S, Tanaka S. Diffusion characteristics of airborne particles with gravitational settling in a convection-dominant indoor flow field. ASHRAE Transactions 1992; 98: 82–97.

[13] Chen F, Yu SCM, Lai ACK. Modeling particle distribution and deposition in indoor environments with a new drift-flux model. Atmos Environ 2006; 40: 357–367.

[14] Zhao B, Chen C, Tan Z. Modeling of ultrafine particle dispersion in indoor environments with an improved drift flux model. J Aerosol Sci 2009; 40: 29–43.

[15] Zhang Z, Chen Q. Experimental measurements and numerical simulations of particle transport and distribution in ventilated rooms. Atmos Environ 2006; 40: 3396–3408.

[16] Zhang Z, Chen X, Mazumdar S, Zhang T, Chen Q. Experimental and numerical investigation of airflow and contaminant transport in an airliner cabin mockup. Build Environ 2009; 44: 85-94.

[17] Chen C, Zhao B. Some questions on dispersion of human exhaled droplets in ventilation room: Answers from numerical investigation. Indoor Air 2010; 20: 95-111.

[18] Wang M, Lin C-H, Chen Q. Advanced turbulence models for predicting particle transport in enclosed environment. Build Environ 2012; 47: 40-49.

[19] Choudhury D. Introduction to the Renormalization Group Method and Turbulence Modeling, Canonsburg, Fluent Inc. Technical Memorandum TM-107. 1993.

[20] Fluent Inc. FLUENT 6.3 Documentation, Fluent Inc., Lebanon, NH. 2005.

[21] Shur M, Spalart P R, Strelets M, Travin A. Detached-Eddy Simulation of an airfoil at high angle of attack. In 4th Int. Symposium on Eng. Turb. Modeling and Experiments, Corsica, France. 1999.
[22] Wang M. Modeling airflow and contaminant transport in enclosed spaces with advanced models. PhD Thesis. Purdue University. 2011.
[23] Gupta JK, Lin C-H, Chen Q. Flow dynamics and characterization of a cough. Indoor Air 2009; 19: 517-525.
[24] Xie X, Li Y, Chwang ATY, Ho PL, Seto WH. How far droplets can move in indoor environments – revisiting the Wells evaporation–falling curve. Indoor Air 2007; 17: 211–225.
[25] ISO 7730. Ergonomics of the thermal environment — Analytical determination and interpretation of thermal comfort using calculation of the PMV and PPD indices and local thermal comfort criteria. Switzerland. 2005.
[26] Liu W, Wen J, Chao J, Yin W, Shen C, Lai D, Lin C-H, Liu J, Sun H, Chen Q. Accurate and high-resolution boundary conditions and flow fields in the first-class cabin of an MD-82 commercial airliner. Atmos Environ 2012; 56: 33-44.
[27] Liu W, Wen J, Shen C, Lin C-H, Liu J, Chen Q. Experimental investigation of air distributions in the first-class cabin of an MD-82 commercial airliner. Proceedings of COBEE, Boulder, CO. 2012.
[28] Hinds WC. Aerosol Technology: Properties, Behavior, and Measurement of Airborne Particles, 2nd edition. New York: Wiley. 1999.
[29] Gupta JK, Lin C-H, Chen Q. Inhalation of expiratory droplets in aircraft cabin. Indoor Air 2011b; 21: 341–350.

Captions of listed figures

Figure 1. Overall calculation procedure.

Figure 2. Airflow field versus room time constant for estimating t_1.

Figure 3. An example of the air velocity versus time at position $s_{\overline{U_m}}$.

Figure 4. Schematic of the office with UFAD system. Air velocity was measured at the seven poles [15].

Figure 5. Schematic of the four-row aircraft cabin mockup [16].

Figure 6. Comparison of air velocities obtained by the different approaches with the experimental data from Zhang and Chen [15].

Figure 7. Comparison of airflow field obtained by the different approaches with the experimental data from Zhang et al. [16]; (a) cross-section through the third row, (b) mid-section along the longitudinal direction.

Figure 8. Jet velocity versus time from DES model and estimated t_2 for (a) office and (b) aircraft cabin case.

Figure 9. Schematic of the fully-occupied first-class cabin: (a) perspective view and (b) plane view [28].

Figure 10. Comparison of 3 independent measurements of particle concentration versus time for (a) 1B and (b) 2A.

Figure 11. Comparison of the particle concentration levels when the source release time was 5, 20 and 60 s for (a) 1A and (b) 2A.

Figure 12. Comparison of the numerical results of transient particle concentration at the breathing zone of each passenger with the corresponding experimental data. The experimental data and modeling results were normalized by the maximum concentration among the monitoring points for the entire experiment.

Figure 13. Comparison of the numerical results of air velocity vectors with the experimental data from Liu et al. [28] at the cross-section through the third row.